JOC Article

A Computational Study on the Mechanism for the Chemical Fixation of Nitric Oxide Leading to 1,2,3-Oxadiazole 3-oxide

Yong Wu,[†] Ying Xue,*[,†] Daiqian Xie,*[,†,‡] and Guosen Yan[†]

College of Chemistry, Key Lab of Green Chemistry and Technology in Ministry of Education, Sichuan University, Chengdu, 610064, P. R. China, and Institute of Theoretical and Computational Chemistry, Laboratory of Mesoscopic Chemistry, Department of Chemistry, Nanjing University, Nanjing 210093, P. R. China

xueyingscu@163.com; dqxie@nju.edu.cn

Received February 17, 2005

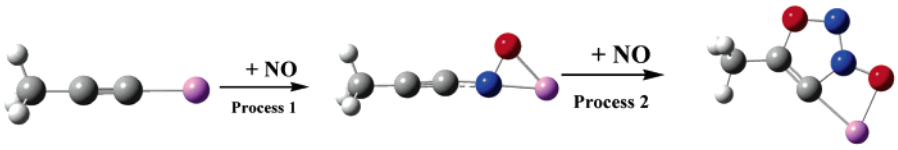

The chemical fixation of nitric oxide (NO) reacting with alkynyllithium to produce 5-methyl-3-oxide-1,2,3-oxadiazole has been investigated by using ab initio (U)MP2 and DFT/(U)B3LYP methods. The solvent effect was assessed using the combination of microsolvation model with explicit THF ligands on lithium and continuum solvent model based on the SCRF/CPCM method at the (U)-B3LYP/6-31G* level. Our results reveal that the overall reaction is stepwise and considered to include two processes. In process 1, the nitrogen atom in nitric oxide at first attacks the C_1 atom in alkynyllithium to afford the intermediate **5**. In process 2, after another nitric oxide reacted with the intermediate **5** to produce **8a**, we found that two pathways are involved. For path 1, the O_2 atom at first attacks the C_2 atom to form a five-membered ring geometry, and then lithium can rotate around the N_1-O_1 bond, leading to the product 5-methyl-3-oxide-1,2,3-oxadiazole followed addition of water. However, for path 2, lithium atom rotates first around the N_1-O_1 bond, and then the product 5-methyl-3-oxide-1,2,3-oxadiazole is also generated by addition of water. Our calculations indicate that path 1 is more favorable than path 2 in the gas phase, while both of them exist possibly in THF solvent. The overall reaction is exothermic.

Introduction

Nitric oxide (NO), as a free radical, is a paramagnetic gas. Recently, the geometrical structures for the dimeric form of $(NO)_2$ have been theoretically investigated using high-level ab initio methods.[1,2] Of these conformers, the *cis* isomer (N−N interaction) is a global minimum. The binding energies and the relative energy gaps between these conformers are found to be relatively small. Although the NO monomer, with an unpaired electron in the nitrogen atom, can combine with the other to form the dimeric structures, the interaction is very weak like a van der Waals complex. Therefore, it is very easy for the dimeric structures to dissociate into the monomer nitric oxide due to the small binding energy.

As we know, nitric oxide is considered to be an atmospheric pollutant along with NO_2, mainly leading to acid rain. On the other hand, nitric oxide has attracted increasing attention in the biological and chemical fields.[3−22] Many studies have shown that NO has a variety of biological activities including inhibition of

[†] Sichuan University.
[‡] Nanjing University.

(1) Park, J. K.; Sun, H. *Chem. Phys.* **2001**, *263*, 61.
(2) Magers, D. H.; Qiong, H.; Leszczýnski, J. *Struct. Chem.* **2002**, *13*, 165.
(3) Stamler, J. S.; Singel, D. J.; Loscalzo, J. *Science* **1992**, *258*, 1898.
(4) Durante, W.; Kroll, M. H.; Vanhoutte, P. M.; Schafer, A. I. *Blood* **1992**, *79*, 110.
(5) Ress, D. D.; Palmer, R. M. J.; Moncada, S. *Proc. Natl. Acad. Sci. U.S.A.* **1989**, *86*, 3375.
(6) Warren, J. B.; Coughlan, M. L.; Williams, T. J. *Br. J. Pharmacol.* **1992**, *106*, 953.
(7) Pfeiffer, S.; Mayer, B.; Hemmens, B. *Angew. Chem., Int. Ed.* **1999**, *38*, 1714.
(8) Murad, F. *Angew. Chem., Int. Ed.* **1999**, *38*, 1856.
(9) Furchgott, R. F. *Angew. Chem., Int. Ed.* **1999**, *38*, 1870.
(10) Ignarro, L. J. *Angew. Chem., Int. Ed.* **1999**, *38*, 1882.
(11) Arulsamy, N.; Bohle, D. S. *Angew. Chem., Int. Ed.* **2002**, *41*, 2089.
(12) Danzig, M. J.; Riccitiello, S. R. *J. Org. Chem.* **1962**, *27*, 686.
(13) Janzen, E. G.; Wilcox, A. L.; Manoharan, V. *J. Org. Chem.* **1993**, *58*, 3597.
(14) Itoh, T.; Nagata, K.; Okada, M.; Ohsawa, A. *Tetrahedron Lett.* **1995**, *36*, 2269.
(15) Itoh, T.; Nagata, K.; Okada, M.; Ohsawa, A. *Tetrahedron Lett.* **1996**, *37*, 4165.

10.1021/jo0503005 CCC: $30.25
Published on Web 05/27/2005

SCHEME 1

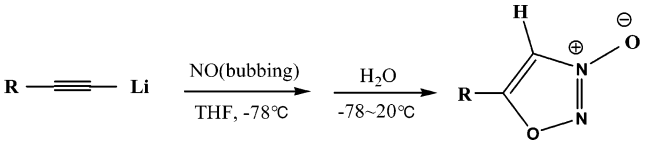

platelet aggregation,[4] relaxation of smooth muscle,[5] neurotransmission, [6] and so on. It is also a unique signaling molecule and a biological messenger in biochemical processes. [7−11] In addition, nitric oxide is also widely used in chemical synthesis.[12−22] Due to the high reactivity of nitric oxide, it is a key component in chemical synthesis for directly fixing nitric oxide into organic molecules in high yield under mild conditions. Recently, Hrabie et al.[21] presented a review on reactions of nitric oxide leading to a special atomic grouping of two nitrogen and two oxygen atoms ($-N_2O_2-$). Although the chemical fixation of nitric oxide was extensively experimentally investigated in the past decades, a new reaction of nitric oxide with alkynes was not reported until last year. Sugihara et al.[22] have investigated the reaction of nitric oxide with various alkynes in a THF solution. The results showed that the yield of product, by using alkynyllithium as the reactant, was dramatically improved and that the reaction was reproducible at −78 °C (Scheme 1). The reaction also offered as reliable candidates 1,2,3-oxadiazole 3-oxides, which are much more stable than 1,2,3-oxadiazoles for drug frameworks.

To the best of our knowledge, the theoretical study on the mechanism of the title reaction has not been reported until now. Thus, in this work, our motif is to clearly clarify the mechanism of the reaction of nitric oxide with alkynyllithium leading to 1,2,3-oxadiazole 3-oxide. To shorten the CPU time and present the general picture of the mechanism, the group R = CH_3 in the alkynyllithium was chosen. We have performed the detailed calculations using the (U)MP2 method to theoretically study this reaction in the gas phase. In addition, the natural bond orbital (NBO) analysis is also carried out to observe the bond order changes in the process of the reaction, and the solvent effect is examined by using the microsolvation and continuum solvent model with the density functional theory (DFT).

Computational Details

The structures of all of the reactants, complexes, transition states, intermediates, and products were fully optimized using the ab initio (U)MP2 method with the standard 6-31G** basis set in our calculations. The harmonic vibrational frequencies were also calculated at the same level to characterize the nature of the stationary points as true minima with no imaginary or transition states with only one imaginary frequency and to provide thermodynamic quantities such as thermal corrections to energy, enthalpy, and Gibbs free energy. All thermodynamic data reported in this paper were estimated at the experimental temperature of −78 °C and pressure of 1.0 atm as presented in ref 22. Wiberg bond indices for all stationary points were analyzed using the natural bond orbital (NBO) method.[23] To refine the energies, single-point energies were calculated at the (U)MP2/6-311++G** level for all stationary points. To match further with the experimental conditions, we also took into account the solvent effect on the reaction. Recently, Pratt et al.[24−26] investigated the solvent effects of some lithium compounds. They reported that a combination of the microsolvation and continuum solvent models was good to examine the solvent effect. Therefore, in this work, the microsolvation model with explicit THF ligands on lithium was used to optimize all relevant stationary points at the (U)B3LYP/6-31G* level, and then the single-point energy calculations were performed by using the conductor-like polarized continuum model (CPCM)[27] at the (U)B3LYP/6-311++G** level to further estimate the solvent effect on the optimized geometries. All calculations mentioned above were carried out using the Gaussian 98 or Gaussian 03 program.[28]

Results and Discussion

Reaction Mechanism in the Gas Phase. In the absence of the THF solvent, all of the relevant stationary points have been located at the (U)MP2/6-31G** level. Our results shed light on that the title reaction should be considered to include two reaction processes (Scheme 2).

Process 1: Formation of Intermediate 5. In process 1, one complex **1**, two transition states **2** and **4**, and two intermediates **3** and **5** have been located at the UMP2/6-31G** level. The corresponding structures are presented in Figure 1. Because nitric oxide is a radical with an unpaired electron in the nitrogen atom, the optimizations for nitric oxide and other relevant structures should be carried out using open-shell systems in this process. Therefore, we performed the UMP2 method in our calculations. However, the wave function is no longer a pure doublet but is contaminated by states of higher spin multiplicity, as reflected in the spin-squared expectation value $\langle S^2 \rangle$ greater than 0.75. In this work, we have checked the values $\langle S^2 \rangle$ for all relevant stationary points and found that the value varies from 0.78 in reactant NO to 0.87 in intermediate **5**. Hence, it is important to note that the electronic energies have been corrected with the use of the projected MP2 (PMP2) method. As shown in Scheme 2 and Figure 1, one can see that process 1 proceeds via three steps. The first step is to form complex **1** via the interaction of the nitrogen in nitric oxide with

(16) Itoh, T.; Nagata, K.; Matsuya, Y.; Miyazaki, M.; Ohsawa, A. *Tetrahedron Lett.* **1997**, *38*, 5017.
(17) Itoh, T.; Nagata, K.; Matsuya, Y.; Miyazaki, M.; Ohsawa, A. *J. Org. Chem.* **1997**, *62*, 3582.
(18) Arnold, E. V.; Keefer, L. K.; Hrabieb, J. A. *Tetrahedron Lett.* **2000**, *41*, 8421.
(19) Bohle, D. S.; Imonigie, J. A. *J. Org. Chem.* **2000**, *65*, 5685.
(20) Hrabie, J. A.; Arnold, E. V.; Citro, M. L.; George, C.; Keefer, L. K. *J. Org. Chem.* **2000**, *65*, 5745.
(21) Hrabie, J. A.; Keefer, L. K. *Chem. Rev.* **2002**, *102*, 1135.
(22) Sugihara, T.; Kuwahara, K.; Wakabayashi, A.; Takao, H.; Imagawa, H.; ishizawa, M. *Chem. Commun.* **2004**, 216.
(23) Reed, E.; Curtiss, L. A.; Weinhold, F. *Chem. Rev.* **1988**, *88*, 899.
(24) Pratt, L. A. *J. Org. Chem.* **2005**, *70*, 2294.
(25) Pratt, L. A.; Mu, R.; Jones, D. R. *J. Org. Chem.* **2005**, *70*, 101.
(26) Pratt, L. A.; Mu, R.; *J. Org. Chem.* **2004**, *69*, 7519.
(27) Barone, V.; Cossi, M. *J. Phys. Chem. A* **1998**, *102*, 1995.
(28) Frisch, M. J.; Trucks, G. W.; Schlegel, H. B.; Scuseria, G. E.; Robb, M. A.; Cheeseman, J. R.; Zakrzewski, V. G.; Montgomery, J. A., Jr.; Stratmann, R. E.; Burant, J. C.; Dapprich, S.; Millam, J. M.; Daniels, A. D.; Kudin, K. N.; Strain, M. C.; Farkas, O.; Tomasi, J.; Barone, V.; Cossi, M.; Cammi, R.; Mennucci, B.; Pomelli, C.; Adamo, C.; Clifford, S.; Ochterski, J.; Petersson, G. A.; Ayala, P. Y.; Cui, Q.; Morokuma, K.; Malick, D. K.; Rabuck, A. D.; Raghavachari, K.; Foresman, J. B.; Cioslowski, J.; Ortiz, J. V.; Stefanov, B. B.; Liu, G.; Liashenko, A.; Piskorz, P.; Komaromi, I.; Gomperts, R.; Martin, R. L.; Fox, D. J.; Keith, T.; Al-Laham, M. A.; Peng, C. Y.; Nanayakkara, A.; Gonzalez, C.; Challacombe, M.; Gill, P. M. W.; Johnson, B.; Chen, W.; Wong, M. W.; Andres, J. L.; Gonzalez, C.; Head-Gordon, M.; Replogle, E. S.; Pople, J. A. *Gaussian 98, Revision A.11.3*, Gaussian, Inc., Pittsburgh, PA, **2002**.

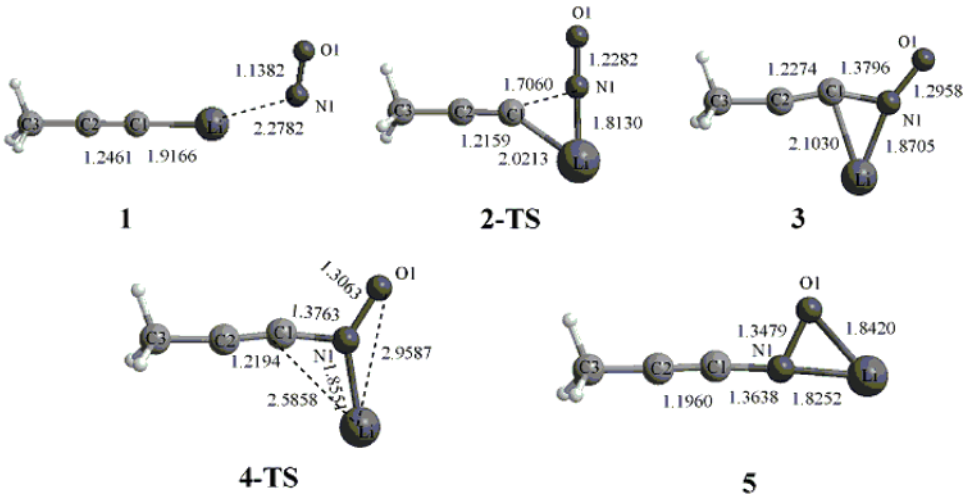

FIGURE 1. Optimized structures in process 1 at the UMP2/6-31G** level.

SCHEME 2

Process 1

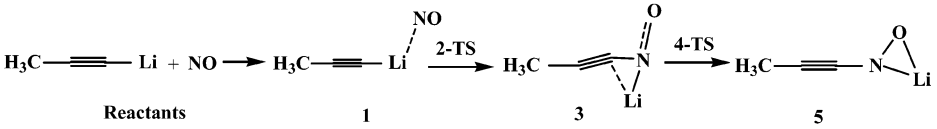

Process 2

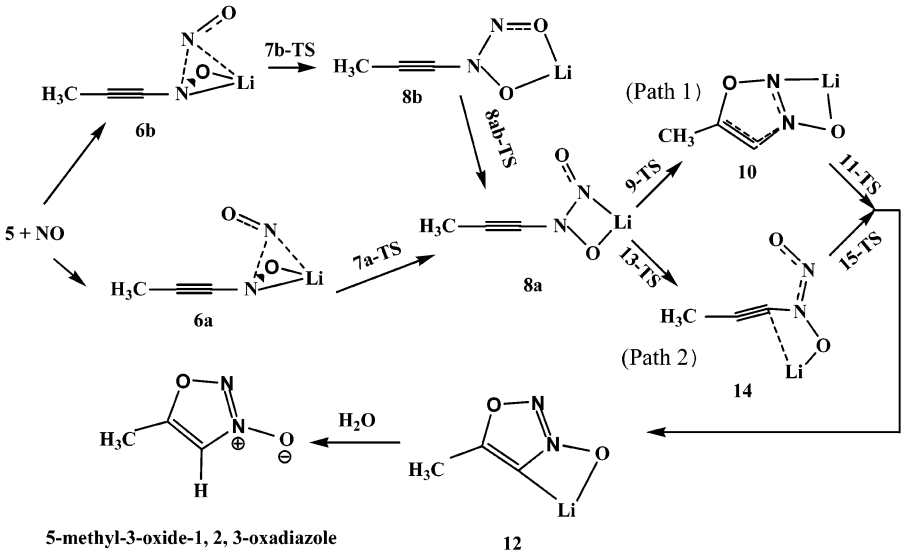

the lithium atom in alkynyllithium; the second step is the attack of nitric oxide to the C_1 atom in alkynyllithium to afford the intermediate **3**; the last step is the rotation of lithium to form **5**. In complex **1**, from Figure 1, the length of the N_1−Li bond is 2.2782 Å. The Wiberg bond index of N_1−Li is 0.1734 with NBO analysis. The binding energy is 5.78 kcal/mol at the UMP2/6-31G** level and 4.23 kcal/mol at the UMP2/6-311++G** level with the thermal correction at −78 °C. In the second step, the transition state **2-TS** has been located at the UMP2/6-31G** level. The lengths of the C_1−N_1, Li−C_1, and Li−N_1 bonds are 1.7060, 2.0213, and 1.8130 Å, respectively. The imaginary frequency is 545.43i cm^{-1}, which is associated with the C_1−N_1 bond stretching motion. The energy barrier from **1** to **2-TS** is 14.33 kcal/mol at the UMP2/6-31G** level and 14.40 kcal/mol at the UMP2/6-311++G** level including the thermal correction at −78 °C. For the intermediate **3**, the lengths of C_1−N_1, Li−C_1, Li−N_1, and N_1−O_1 bonds are 1.3796, 2.1030, 1.8705, and 1.2958 Å, respectively. The values of the Wiberg bond indices in **2-TS** are close to those in **3**, indicating that the transition state **2-TS** is like the intermediate **3**, named as a product-like transition state. Furthermore, N_1−C_1 and N_1−O_1 bond indices are 1.1904 and 1.2383 in **3**, which implies that the N_1−C_1 bond has been completely formed and the N_1−O_1 double bond has been partly broken. In the last step, the transition state **4-TS** has been located at the UMP2/6-31G** level. Its imaginary frequency is 15.094i cm^{-1}, associated with the rotation of Li−N_1 bond in the plane. The lengths of Li−

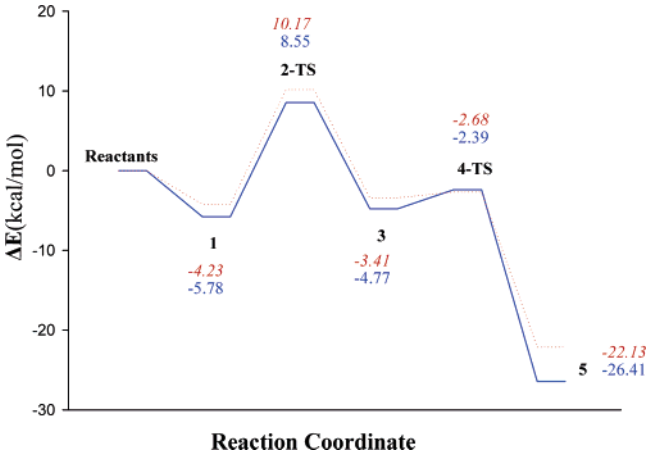

FIGURE 2. Schematic potential energy profiles in process 1 in the gas phase: ΔE (UMP2/6-31G**), blue, solid line; ΔE (UMP2/6-311++G**), red, dashed line.

C_1 and Li−O_1 bonds are 2.5858 and 2.9587 Å, respectively. The energy barrier from **3** to **4-TS** is 2.38 kcal/mol at the UMP2/6-31G** level and 0.73 kcal/mol at the UMP2/6-311++G** level including the thermal correction at −78 °C. For intermediate **5**, the lengths of Li−N_1 and Li−O_1 are 1.8252 and 1.8420 Å, respectively. Our calculations show that the energy dramatically decreases from the intermediate **3** to **5** by ca. 18 kcal/mol in the third step.

The schematic potential energy profiles for process 1 are presented in Figure 2. One can see that the energy decreases from the reactants to the intermediate **5**, which implies that the process is exothermic. Results indicate that step 2 is the rate-limited step in this process.

Process 2: Formation of the Product 5-Methyl-3-oxide-1,2,3-oxadiazole. In this process, the optimized structures are presented in Figures 3−5. After formation of intermediate **5**, we further investigated the reaction process of another nitric oxide with intermediate **5**. In our calculations, as shown in Figure 3, two possible complexes (**6a** and **6b**) were located at the MP2/6-31G** level. For complex **6a**, the lengths of the Li−N_2 and N_1−N_2 bonds are 1.4576 and 2.1991 Å, respectively. The binding energy is 16.09 kcal/mol at the MP2/6-31G** level and 12.30 kcal/mol at the MP2/6-311++G** level including the thermal correction at −78 °C. Then, the N_2 atom can attack the N_1 atom to form the N_1−N_2 bond. In this step, the transition state **7a-TS** has been located at the MP2/6-31G** level. The N_1−N_2 distance is 1.7830 Å, which is 0.4161 Å shorter than that in **6a**. The Li−N_2 distance is 3.1260 Å, which is 1.6684 Å longer than that in **6a**. The imaginary frequency is 160.28i cm^{-1}, which is associated with N_1−N_2 bond stretching motion. The energy barrier from **6a** to **7a-TS** is 10.20 kcal/mol at the MP2/6-31G** level and 7.98 kcal/mol at the MP2/6-311++G** level including the thermal correction at −78 °C. After the reaction surmounted the transition state **7a-TS**, intermediate **8a** is formed. For intermediate **8a**, the O_1, N_1, N_2, O_2, Li, C_1, C_2, and C_3 atoms are almost on the same plane. The Li−O_1, Li−N_1, and N_1−N_2 distances are 1.8381, 2.0806, and 1.3356 Å, respectively. Wiberg bond indices of N_1−N_2 and N_2−O_2 are 1.3376 and 1.5713, which implies that the N_1−N_2 bond has been completely come into being and somewhat conjugated with each other, and that the N_2−O_2 double bond has been partly broken.

On the other hand, for the complex **6b**, the lengths of N_1−N_2, Li−N_1, Li−O_1, and O_1−O_2 are 2.2863, 1.8447, 1.8149, and 2.1557 Å, respectively. It is important to note that the O_2−N_2−N_1−O_1 dihedral angle is −2.47°, which implies that O_1 and O_2 are on the same side. The binding energy is 12.89 kcal/mol at the MP2/6-31G** level and

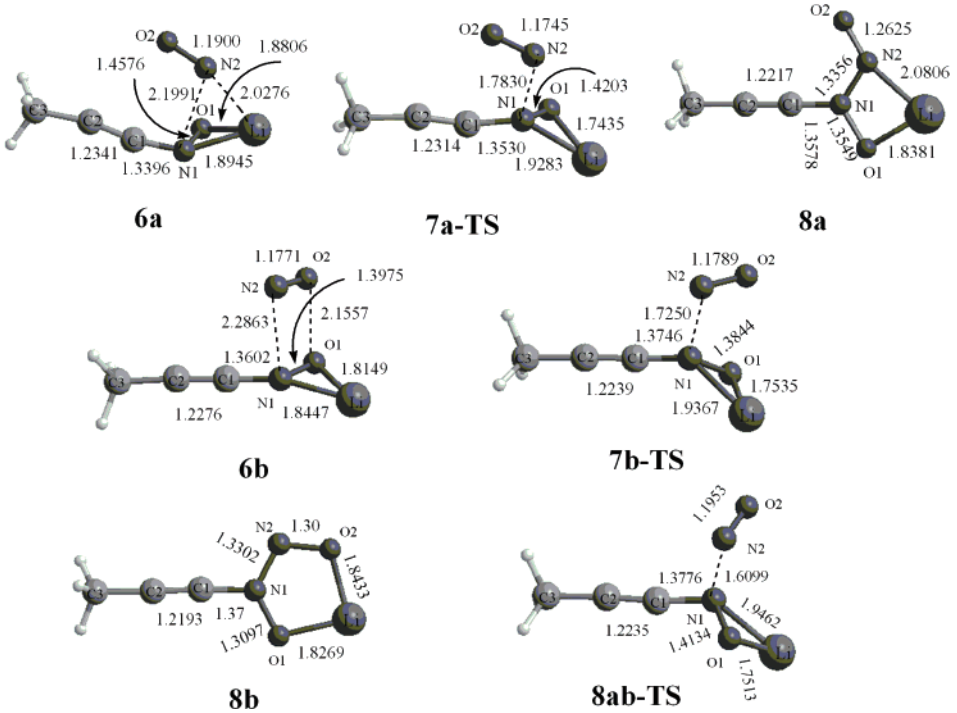

FIGURE 3. Optimized stationary points of **6a**,**b**, **7a-TS**, 7**b-TS**, **8a**,**b**, and **8ab-TS** in process 2 at the MP2/6-31G** level.

9.92 kcal/mol at the MP2/6-311++G** level including the thermal correction at −78 °C. Similar to transition state **7a-TS**, we also located a transition state **7b-TS**, which also corresponds to the formation of the N_1-N_2 bond. The lengths of N_1-N_2 and O_1-O_2 are 1.7250 and 2.4625 Å, which are 0.5613 Å shorter and 0.3068 Å longer than those in the complex **6b.** The imaginary frequency is 238.84i cm^{-1}, which is also associated with the N_1-N_2 bond stretching motion. The energy barrier from **6b** to **7b-TS** is 3.2 kcal/mol at the MP2/6-31G** level and 1.87 kcal/mol at the MP2/6-311++G** level including the thermal correction at −78 °C. The geometry **8b** would be generated if the reaction surpassed the transition state **7b-TS**. For **8b**, as shown in Figure 3, one can see that the lithium atom both interacts with the O_1 and O_2 atom. The lengths of N_1-N_2, $Li-O_1$, $Li-O_2$ and N_1-O_1 are 2.3302, 1.8269, 1.8433 and 1.3097 Å, respectively. The calculated energies indicate that **8b** is ca. 21 kcal/mol lower that that of **8a**. That is to say, if **8b** isomerizes to **8a**, the energy barriers would be no less than ca. 21 kcal/mol. To describe the isomerization process from **8b** to **8a**, the transition state **8ab-TS** was located at the MP2/6-31G** level. In **8ab-TS**, the lengths of $Li-N_1$, $Li-O_1$, O_1-N_1, N_2-O_2, and N_1-N_2 are 1.9462, 1.7513, 1.4134, 1.1953, and 1.6099 Å, respectively. Note that the $O_2-N_2-N_1-C_1$ dihedral angle is −104.87°. The imaginary frequency is 96.96i cm^{-1}, which is associated with the N_1-N_2 bond rotation mode. Our calculations show that the energy barrier from **8b** to **8a** is 42.07 kcal/mol at the MP2/6-31G** and 40.23 kcal/mol at the MP2/6-311++G** level including the thermal correction at −78 °C, respectively. It is implied that the isomerization process from **8b** to **8a** is very difficult in the reaction. Moreover, as mentioned above, **6a** is more stable than **6b** because the binding energy of **6a** is higher than that of **6b**. Therefore, in this work, it is rational to form the complex **6a** and to generate the intermediate **8a,** and then the reaction goes on.

In the next section,two possible pathways, leading to the product 5-methyl-3-oxide-1,2,3-oxadiazole, have been investigated. One is that the O_2 atom directly attacks the C_2 atom; the other is that the O_2 atom also attacks the C_2 atom after the torsion of lithium around the N_1-O_1 bond about 180°. We denote the two pathways as path 1 and path 2 in our calculations.

Path 1. As shown in Figure 4, we at first have located the transition state **9-TS** at the MP2/6-31G** level, which directly connects with the intermediates **8a** and **10**. For **9-TS**, the C_2-O_2, C_1-C_2, and O_2-N_2 distances are 2.2108, 1.2520, and 1.2804 Å, respectively. The $C_2-C_1-N_1$ bond angle is 124.1°. It is indicated that the transition state **9-TS** has the trend to produce a five-membered-ring geometry. The imaginary frequency is 261.9i cm^{-1}. The analysis of the vibrational modes indicates that this imaginary frequency is associated with the O_2-C_2 bond stretching motion. Wiberg bond indices show that the transition state **9-TS** is a reactant-like geometry due to the small differences between **8** and **9-TS**. The calculated energy barrier from **8** to the transition state **9-TS** is 5.93 kcal/mol at the MP2/6-31G** level and 7.35 kcal/mol at the MP2/6-311++G** including the thermal correction at −78 °C. For the intermediate **10**, Wiberg bond indices of C_1-C_2, O_2-C_2, and N_2-O_2 bonds change from 2.7583, 0.0366, and 1.5713 in **8** to 1.5435, 0.9829, and 1.0686 in **10.** The C_1-C_2 and N_2-O_2 distances are 1.3826 and 1.3469 Å in **10**, which are 0.0248 and 0.0844 Å longer than those in **8.** The O_2-C_2 distance is 1.4014 Å. It is revealed that the C_1-C_2 and N_2-O_2 bonds are weakened while the O_2-C_2 bond possesses single-bond nature. We suppose that the lithium atom can rotate about 180° around the C_1-O_1 bond to interact with the electronegative C_1 atom. To verify this supposition, we have located the transition state **11-TS** at the MP2/6-31G** level. The $C_1-N_1-O_1-Li$ dihedral angle is 100.6°; the imaginary frequency is 153.09i cm^{-1}, which exactly corresponds to the torsion of lithium atom around the N_1-O_1 bond. The energy barrier from **10** to **11-TS** is 4.99 kcal/mol at the MP2/6-31G** level and 5.71 kcal/mol at 6-311++G** level with the thermal correction at −78 °C. After the reaction overcame the transition state **11-TS**, the geometry **12** is produced. In **12**, the $Li-C_2$ and $Li-O_1$ distances are 2.0710 and 1.8809 Å. Note that the Li, C_1, C_2, O_1, O_2, N_1, N_2, and C_3 atoms are also almost on the same plane. Our results show that the energy of **12** is ca. 15 kcal/mol lower than that of **10**. In view of the energy barrier and relative energy between **10** and **12**, it is very favorable for the torsion of lithium atom around the N_1-O_1 bond to proceed via the transition state **11-TS** in the gas phase.

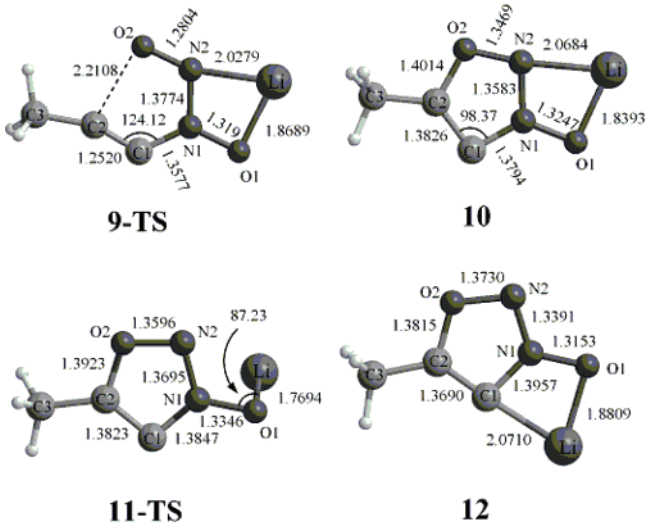

FIGURE 4. Optimized geometries in path 1 of process 2 at the MP2/6-31G** level.

Path 2. We also found that the lithium atom can rotate around the N_1-O_1 bond in **8**. As shown in Figure 5, the transition state **13-TS** has been located in this rotation step. The $C_1-N_1-O_1-Li$ dihedral angle is 66.9°; the imaginary frequency is 103.53i cm^{-1}, which is also corresponded to the lithium atom rotation mode. The energy barrier from **8** to **13-TS** is 12.52 kcal/mol at the MP2/6-31G** level and 13.63 kcal/mol at the MP2/6-311++G** level with the thermal correction at −78 °C. In view of the energies, the energy barrier in this step is about 3.5 higher than that in the step of **8** to **10**, which indicates that this step of the lithium atom rotation is somewhat more difficult than the step of **8** to **10**. If the reaction surmounted the transition state **13-TS**, it would generate the intermediate **14** in our calculations. In **14**, as shown in Figure 5, the $Li-C_1$ and $Li-O_1$ are 2.3207 and 1.7769 Å, respectively. It should be noted that the Li, C_1, C_2, O_1, O_2, N_1, N_2, and C_3 atoms are also almost

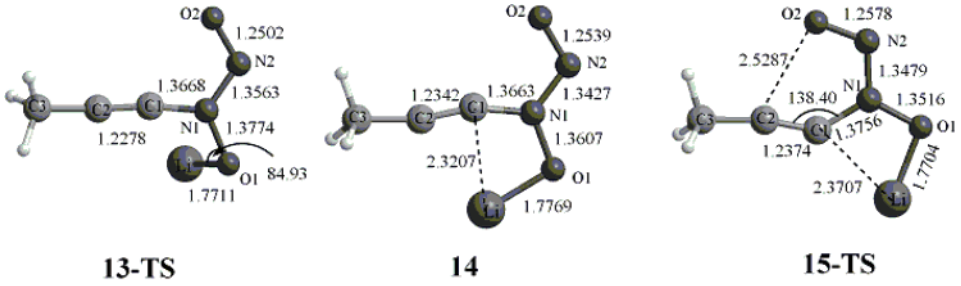

FIGURE 5. Optimized geometries in path 2 of process 2 at the MP2/6-31G** level.

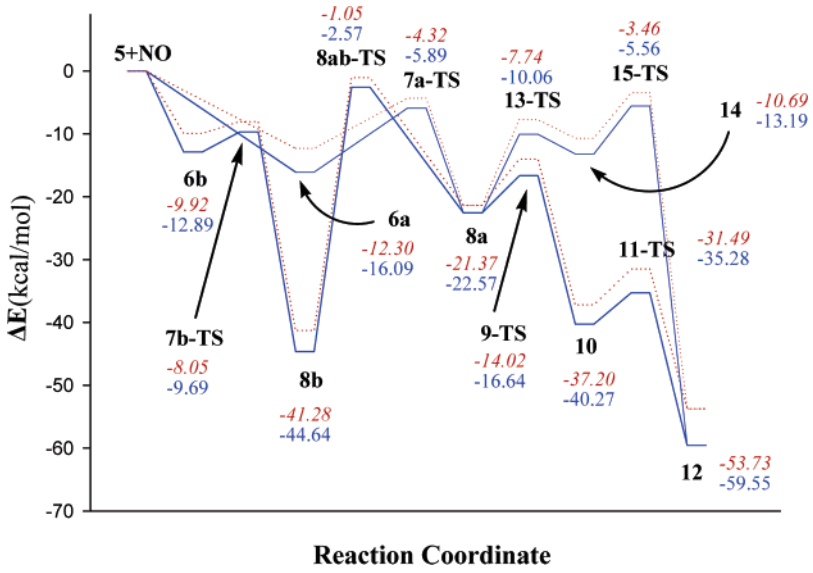

FIGURE 6. Schematic potential energy profiles in process 2 in the gas phase: ΔE (MP2/6-31G**), blue, solid line; ΔE (MP2/6-311++G**), red, dashed line.

on the same plane. And then, the transition state **15-TS**, associated with the attack of the O_2 atom to the C_2 atom, has been located at the MP2/6-31G** level. The O_2-C_2 distance is 2.5287 Å. The imaginary frequency is 179.07i cm^{-1}, which is associated with the O_2-C_2 bond-stretching mode. The Wiberg bond indices indicate that the transition state **15-TS** is a reactant-like geometry. The energy barrier from **14** to **15-TS** is 7.63 kcal/mol at the MP2/6-31G** level and 7.23 kcal/mol at the MP2/6-311++G** level with the thermal correction at −78 °C. Next, the geometry **12** is also generated after the reaction surmounted the transition state **15-TS**.

In addition, the schematic potential energy profiles for process 2 are presented in Figure 6. One can see that the energy is also downhill and that path 1 is more favorable than path 2. Accordingly, this process is exothermic and stepwise.

Reaction Mechanism in THF. To estimate the solvent effect of THF on the title reaction, we reoptimized the geometries based on the microsolvation model by using two THF ligands on the lithium atom at the B3LYP/6-31G* level, and then single-point energies were calculated for the optimized geometries at the B3LYP/6-311++G** level by using the SCRF method based on the CPCM model in solvent THF. The optimized molecular structures and energies of all stationary points along the reaction paths in THF are given in Figure S-1 and Tables S-2 and S-5 of the Supporting Information.

Process 1. Although spin contamination exists in these geometries, our results were not corrected by using the projected method because $\langle S^2 \rangle$ slightly deviates from 0.75, varying from 0.7525 in nitric oxide to 0.7636 in **S3**. For the complex **S1**, the lengths of $Li-N_1$, N_1-C_1, and $Li-C_1$ are 2.1752, 2.5039, and 2.0066 Å, respectively. The binding energy is 5.93 kcal/mol at the UB3LYP/6-31G* level with the thermal correction at −78 °C. For the transition state **S2-TS**, the lengths of N_1-C_1, $Li-C_1$, and $Li-N_1$ are 1.7904, 2.1155, and 1.9297 Å. the imaginary frequency is 345.36i cm^{-1}, which is associated with the N_1-C_1 bond-stretching mode. The calculated energy barrier is 4.24 kcal/mol at the UB3LYP/6-31G* level with the thermal correction at −78 °C. For intermediate **S3**, the N_1-C_1 bond has completely formed. The lengths of N_1-C_1, $Li-N_1$, and $Li-O_1$ are 1.3285, 1.9430, and 1.8537 Å. For this process, the potential energy profile is presented in Figure 7I. Compared with the results in the gas phase, the explicit THF ligands remarkably affect the reaction. As shown in Figure 7I, there is only one transition state, which indicates that the transition state **3-TS** located in the gas phase is not stable in THF.

Furthermore, we also carried out the SCRF calculations on the basis of the CPCM model for process 1. Our calculations exhibit that the energy barrier of the transition state **S2-TS** is dramatically decreased to 2.54 kcal/mol.

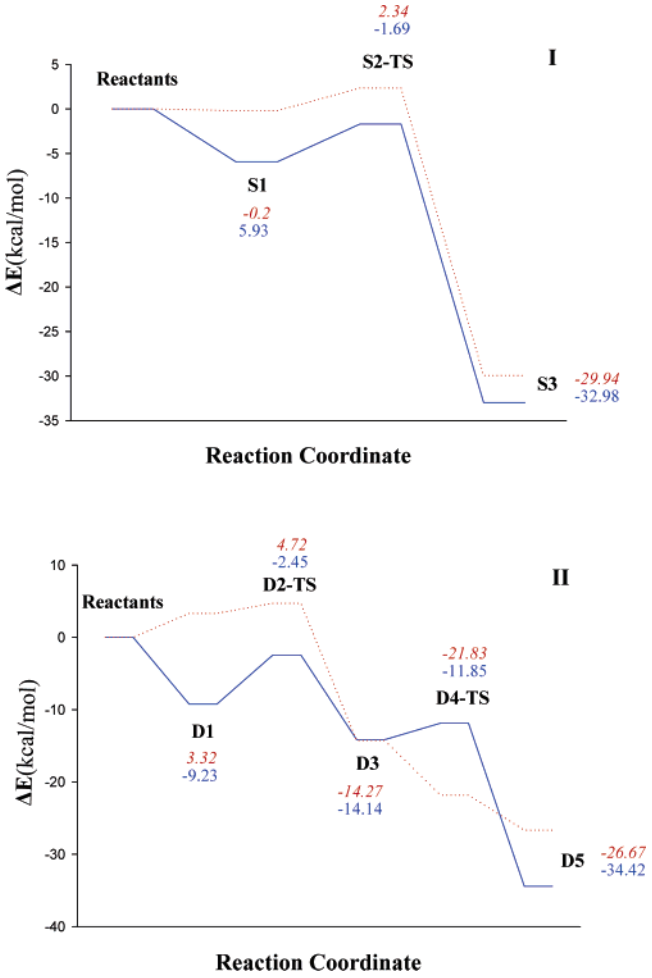

FIGURE 7. Schematic potential energy profiles in process 1: I, with two explicit THF; II, without explicit THF; Δ*E* (UB3LYP/6-31G*), blue, solid line; Δ*E* (SCRF/UB3LYP/6-311++G**), red, dashed line.

Process 2. Due to the steric effect of THF ligands on lithium, we cannot locate any minimum like **6a** or **6b**. In our work, like **8a** and **8b**, we have located the minima **S4a** and **S4b** at the B3LYP/6-31G* level. For **S4a**, the $O_2-N_2-N_1-O_1$ dihedral angle is about 180°; the lengths of $Li-O_1$ and $Li-N_2$ are 1.8948 and 2.2013 Å, respectively. The binding energy is 17.35 kcal/mol at the B3LYP/6-31G* level with the thermal correction at −78 °C. For **S4b**, the $O_2-N_2-N_1-O_1$ dihedral angle is about 0°, the lengths of $Li-O_1$ and $Li-O_2$ are 1.8798 and 1.9232 Å, and the binding energy is 33.81 kcal/mol at the B3LYP/6-31G* level with the thermal correction at −78 °C.

Similar to the results in the gas phase, we also have investigated two pathways in THF in our study. In path 1, for the transition state **S5-TS**, the O_2-C_2 distance is 2.1827 Å; the imaginary frequency is 212.38i cm^{-1}, which is associated with the O_2-C_2 bond-stretching mode. The energy barrier is 7.03 kcal/mol at the B3LYP/6-31G* level with the thermal correction at −78 °C. For **S6**, it is generated after the reaction surmounted the transition state **S5-TS**. The lengths of $Li-N_2$ and Li−O1 are 2.2883 and 1.8801 Å, respectively; The O_2-C_2 distance is 1.3861 Å, which implies that the O_2-C_2 bond has completely formed. Note that the $Li-O_1-N_1-N_2$ dihedral angle is −140.40°, different from that in **10** in the gas phase. According to the results in the gas phase, like **10** and **12**, lithium attaching to the C_1 atom is more stable than that attaching to the N_2 atom. It is possible for **S6** to rotate the N_1-O_1 bond, leading to **S8** in the reaction. Therefore, we have optimized **S8** and found its energy is 12.99 kcal/mol lower than that of **S6** at the B3LYP/6-31G* level with thermal correction at −78 °C. For **S8**, the lengths of $Li-C_1$ and $Li-O_1$ are 2.1633 and 1.9671 Å, respectively; the lithium atom is almost on the plane of the five-member ring. Then, the transition state **S7-TS**, which direct connects **S6** and **S8,** has been located at the B3LYP/6-31G* level. For the **S7-TS**, the $Li-O_1-N_1-C_1$ dihedral angle is −119.15°; the lengths of $Li-N_2$ and $Li-O_1$ are 2.7894 and 1.8326 Å, respectively. The imaginary frequency is 43.76i cm^{-1}, which is associated with the rotation mode of the five-membered ring around the N_1-O_1 bond. The energy barrier is 0.07 kcal/mol. The results imply that the transition state **S7-TS** is very close to **S6** and that it is very favorable to produce **S8**.

In path 2, we at first planned to optimize a transition state like **13-TS**. Unfortunately, this transition state cannot located due to the two explicit THF ligands on the lithium atom. For the intermediate **S9,** the lengths of $Li-C_1$ and $Li-O_1$ are 2.6278 and 1.8228 Å. the $Li-O_1-N_1-C_1$ dihedral angle is −11.98°, which indicates that Li atom slightly deviates the plane. For the transition state **S10-TS**, the length of $Li-C_1$ is 2.5902 Å, which is 0.0376 Å shorter than that in **S9**; the length of O_2-C_2 is 2.5888 Å. the imaginary frequency is 135.12i cm^{-1}, which is also associated with the O_2-C_2 bond stretching mode. The energy barrier is 3.21 kcal/mol at the B3LYP/6-31G* level including thermal correction at −78 °C. After the reaction surmounted the transition state **S10-TS**, it also can offer the geometry **S8**.

Finally, we also perform the SCRF calculation based on the CPCM model at the B3LYP/6-311++G** level for process 2. In our work, the SCRF calculations increase the energy barriers of **S5-TS** to 10.03 kcal/mol, **S7-TS** to 0.88 kcal/mol, and **S10-TS** to 4.4 kcal/mol. It turned out that the SCRF calculations little affect the results obtained by using the microsolvation model in process 2. In addition, the energies of the transition state **S5-TS** and **S10-TS** are very close, which implied that paths 1 and 2 both possibly exist in the reaction in THF. As shown in Figure 8I, one can see that, like in the gas phase, the energy is downhill and this process is exothermic and stepwise in the THF solvent.

In addition, to compare with the results calculated by using microsolvation method at the B3LYP/6-31G* level, we have also investigated the reaction without the explicit THF ligands on the lithium atom at the same level. The results are also presented in Figures 7II and 8II. We checked all stationary points optimized at the B3LYP/6-31G* level and found that the geometry parameters are very close to these calculated at the MP2/6-31G** level except the complex **1**. As shown in Figure 7II, one can see that the solvent remarkably affects process 1. The energy barrier of the step from D3 to D5 is 2.29 kcal/mol in the gas phase. However, the energy barrier disappears including the solvent effect, which is very agreement with the result obtained by using microsolvation model. For process 2, as shown in Figure 8II, the results also exhibit that this process is stepwise and

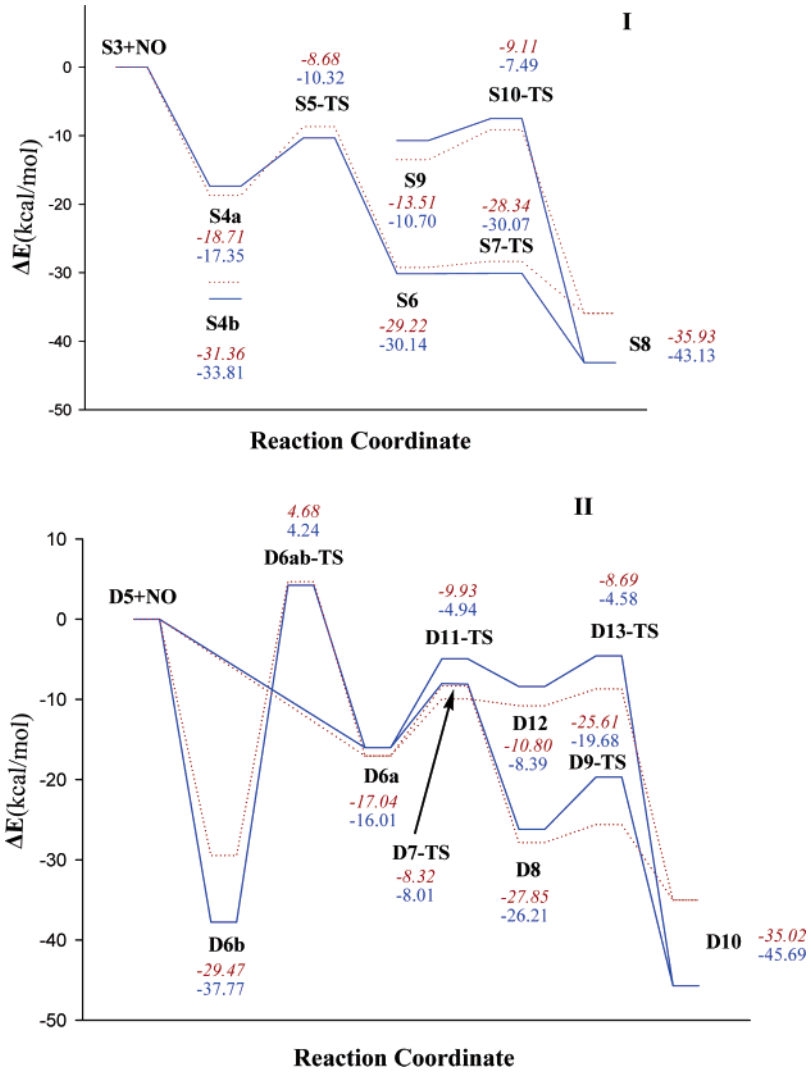

FIGURE 8. Schematic potential energy profiles in process 2: I, with two explicit THF; II, without the explicit THF; Δ*E* (B3LYP/6-31G*), blue, solid line; Δ*E* (SCRF/B3LYP/6-311++G**), red, dashed line).

exothermic. The energy barrier of **D6ab-TS** is 34.15 and 42.01 kcal/mol with and without solvent effect, which also implies that the isomerization from **D6b** to **D6a** is very difficult. The energy barrier of **D11-TS** is 7.11 and 11.07 kcal/mol with and without the solvent effect in path 2, while the energy barrier of **D7-TS** is 8.72 and 8.0 kcal/mol with and without the solvent effect in path 1. It is implied that path 2 is also favorable to proceed in this process. The information supports and makes up the results obtained by using the microsolvation model.

Analysis of 5-Methyl-3-oxide-1,2,3-oxadiazole. To the end, the product 5-methyl-3-oxide-1,2,3-oxadiazole can be generated by addition of water after the reaction afforded the intermediate **12** in the overall reaction. Its geometry was optimized at the MP2/6-311++G** level, and vibrational analysis was also performed at the same level in our calculations. The results are presented in Figures 9 and 10, respectively. It is important to note that the product 5-methyl-3-oxide-1,2,3-oxadiazole has C_s symmetry. As shown in Figure 10, the calculated IR spectrum has a very strong peak whose intensity is much bigger than those of others. Moreover, we checked the vibrational modes and found that this strong line is associated with the N_1-O_1 bond stretching mode. To

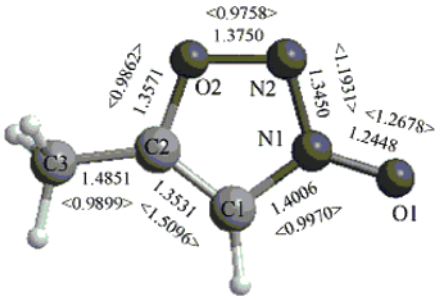

FIGURE 9. Optimized geometry and bond indices of 5-methyl-3-oxide-1,2,3-oxadiazole at the MP2/6-311++G** level.

obtain more information regarding the vibrational modes, we also calculated the Raman spectrum for 5-methyl-3-oxide-1,2,3-oxadiazole in this work, shown in Figure 10. Different from the IR spectrum, five stronger peaks occur in the Raman spectrum. The results show that the Raman spectrum not only presents the N_1-O_1 bond stretching mode but also presents the stretching modes of the $C_1=C_2$, C_1-H, and two C−H bonds in CH_3 group. The frequencies of the ν_{C1-H}, ν_{N1-O1}, and $\nu_{C1=C2}$ modes are 3341, 1639, and 1699 cm^{-1}. Note that the activity of the

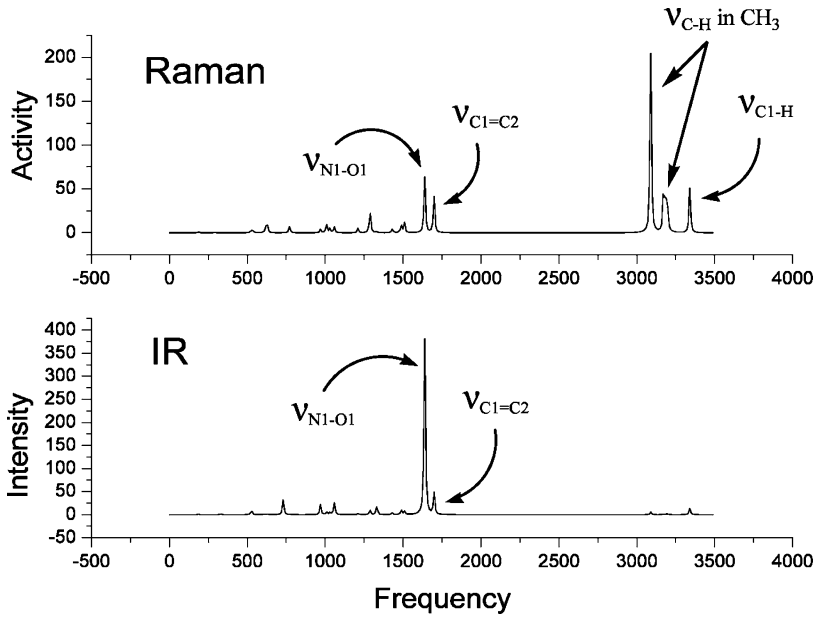

FIGURE 10. Calculated IR and Raman spectra of 5-methyl-3-oxide-1,2,3-oxadiazole at the MP2/6-311++G** level (frequency, cm^{-1}; intensity, km/mol; activity, $Å^4$/amu).

TABLE 1. Calculated Excited States of 5-Methyl-3-oxide-1,2,3-oxadiazole at the MP2/6-311++G Level**

exited state	symmetry	excited energy (eV)	oscillator strength (f)	assignment
1	triplet-A′	2.3616	0	26 → 27 (+149%), 26 → 29 (+9%), 24 → 27 (+6%)
2	triplet-A″	4.0532	0	25 → 27 (+99%), 25 → 29 (+5%)
3	singlet-A″	4.4381	0.0005	25 → 27 (+93%)
4	triplet-A′	4.4405	0	24 → 27 (+101%), 24 → 29 (12%)
5	singlet-A′	5.0312	0.06	26 → 27 (+64%), 26 → 29 (15%)
6	triplet-A′	5.1947	0	26 → 29 (+91%)
7	triplet-A″	5.7292	0	26 → 28 (+97%)
8	triplet-A′	5.7481	0	24 → 29 (+93%), 24 → 27 (+8%), 24 → 32 (6%)
9	singlet-A″	5.7556	0.0005	26 → 28 (+98%)
10	singlet-A′	5.8807	0.0363	26 → 29 (+58%), 24 → 27 (+18%), 26 → 27 (+9%)
11	triplet-A″	5.9331	0	23 → 27 (+98%), 25 → 29 (6%)
12	triplet-A″	6.1479	0	25 → 29 (+87%), 23 → 27 (+6%), 25 → 27 (5%)
13	singlet-A′	6.1673	0.2572	24 → 27 (+61%), 26 → 29 (19%)
14	singlet-A″	6.2382	0.0007	25 → 29 (+93%)
15	triplet-A″	6.4649	0	26 → 30 (+74%), 26 → 31 (+12%), 26 → 33 (+8%),
16	singlet-A″	6.5127	0.0001	26 → 30 (+92%)
17	triplet-A′	6.5608	0	25 → 28 (+97%)
18	singlet-A′	6.5896	0.0181	25 → 28 (+95%)
19	singlet-A″	6.7715	0.0001	26 → 31 (+75%), 26 → 34 (6%), 23 → 27 (+6%), 26 → 30 (6%),
20	singlet-A″	6.9532	0.0073	23 → 27 (+60%), 24 → 28 (23%), 26 → 31 (8%)

ν_{N1-O1} mode is almost equal to that of the $\nu_{C1=C2}$ mode in Raman spectrum.

In addition, to theoretically study the absorption spectrum of 5-methyl-3-oxide-1,2,3-oxadiazole, the time-dependent (TD) B3LYP calculation with 6-311++G** basis set was employed on the geometry calculated at the MP2/6-311++G** level. As shown in Table 1, 10 singlet states and 10 triplet states were calculated in this work. The data were further processed using the SWizard program (revision 2.9).[29] In this process, the Gaussian model was used and the half-bandwidths were taken to be equal to 3000 cm^{-1}. Therefore, the absorption spectrum is plotted in Figure 11. One can see that two obvious peaks appear in the absorption spectrum. The strong peak occurs at ca. 6.17 eV (4.98×10^4 cm^{-1}), and the other weak peak is ca. 5.03 eV (4.06×10^4 cm^{-1}). As shown in Table 1, the two peaks, corresponding to the excited states 5 and 10, are all mainly concerned with the orbitals 24, 26, 27, and 29. The weak peak is mainly associated with the transition of 26 to 27, while the strong peak is mainly associated with the transition of 24 to 27. Furthermore, the orbital coefficients reveal that the orbitals 24 and 26 are the C_1=C_2 and N_1=N_2 π orbitals, while that the orbitals 27 and 29 are the C_1=C_2 and N_1=N_2 π^* orbitals, respectively. Correspondingly, the weak peak should be mainly assigned to the $\pi^*_{N1=N2} \leftarrow \pi_{N1=N2}$ transition, while the strong peak should be mainly assigned to the $\pi^*_{N1=N2} \leftarrow \pi_{C1=C2}$ transition.

(29) Gorelsky, S. I. *SWizard program*, http://www.sg-chem.net/.

Conclusions

In this work, the chemical fixation of nitric oxide to produce 5-methyl-3-oxide-1,2,3-oxadiazole has been investigated by using ab inito (U)MP2 and DFT/(U)B3LYP method. The combination of the microslovation model by

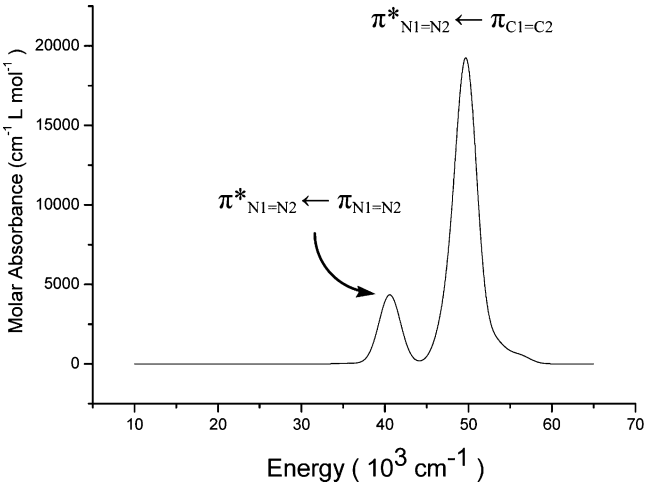

FIGURE 11. Calculated absorption spectrum of 5-methyl-3-oxide-1,2,3-oxadiazole at the MP2/6-311++G** level.

using two explicit THF lingands on the lithium atom and continuum solvent model based on the SCRF/CPCM method was used. Our findings are summarized as follows:

1. The title reaction is stepwise and exothermic.

2. In process 1, the nitrogen atom in nitric oxide attacks the C_1 atom in alkynyllithium to afford the intermediate **5**.

3. In process 1, taken into account the solvent effect, the intermediate **3** can directly transform to the intermediate **5** without energy barrier in THF.

4. In process 2, the intermediate **12** is produced via two pathways, and then the five-member-ring product 5-methyl-3-oxide-1,2,3-oxadiazole is generated by addition of water.

5. In process 2, path 1 is more favorable than path 2 in the gas phase, while they both possible exist in the THF solvent.

6. The analysis of the product 5-methyl-3-oxide-1,2,3-oxadiazole indicates that the strongest IR peak is associated with the N_1-O_1 bond stretching mode and that the strong absorption peak is assigned to the $\pi^*_{N1=N2} \leftarrow \pi_{C1=C2}$ transition.

Acknowledgment. This project has been supported by the National Natural Science Foundation of China (Grant No. 20473055) and the Teaching and Research Award Program for Outstanding Young Teachers in Higher Education Institutions of MOE, China.

Supporting Information Available: Optimized Cartesian coordinates, Tables S-1−S-6 listing energies for all relevant geometries, Figure S-1 showing the geometries by using the microsolvation model at the (U)B3LYP/6-31G* level, and Table S-7 listing the bond indices at the (U)MP2/6-31G** level. This material is available free of charge via the Internet at http://pubs.acs.org.

JO0503005